RESEARCH

Open Access

Establishment of human hematopoietic organoids for evaluation of hematopoietic injury and regeneration effect

Keyi Chen[1,2,3†], Yunqiao Li[3†], Xumin Wu[3], Xuan Tang[1,2,3], Bowen Zhang[3], Tao Fan[3], Lijuan He[3], Xuetao Pei[3*] and Yanhua Li[3*]

Abstract

Background Human hematopoietic organoids have a wide application value for modeling human bone marrow diseases, such as acute hematopoietic radiation injury. However, the manufacturing of human hematopoietic organoids is an unaddressed challenge because of the complexity of hematopoietic tissues.

Methods To manufacture hematopoietic organoids, we obtained CD34$^+$ hematopoietic stem and progenitor cells (HSPCs) from human embryonic stem cells (hESCs) using stepwise induction and immunomagnetic bead-sorting. We then mixed these CD34$^+$ HSPCs with niche-related cells in Gelatin-methacryloyl (GelMA) to form a three-dimensional (3D) hematopoietic organoid. Additionally, we investigated the effects of radiation damage and response to granulocyte colony-stimulating factor (G-CSF) in hematopoietic organoids.

Results The GelMA hydrogel maintained the undifferentiated state of hESCs-derived HSPCs by reducing intracellular reactive oxygen species (ROS) levels. The established hematopoietic organoids in GelMA with niche-related cells were composed of HSPCs and multilineage blood cells and demonstrated the adherence of hematopoietic cells to niche cells. Notably, these hematopoietic organoids exhibited radiation-induced hematopoietic cell injury effect, including increased intracellular ROS levels, γ-H2AX positive cell percentages, and hematopoietic cell apoptosis percentages. Moreover, G-CSF supplementation in the culture medium significantly improved the survival of HSPCs and enhanced myeloid cell regeneration in these hematopoietic organoids after radiation.

Conclusions These findings substantiate the successful manufacture of a preliminary 3D hematopoietic organoid from hESCs-derived HSPCs, which was utilized for modeling hematopoietic radiation injury and assessing the radiation-mitigating effects of G-CSF in vitro. Our study provides opportunities to further aid in the standard and scalable production of hematopoietic organoids for disease modeling and drug testing.

Keywords Hematopoietic stem/progenitor cells, Hematopoietic organoids, Gelatin-methacryloyl, Radiation injury, Granulocyte colony-stimulating factor

---

†Keyi Chen and Yunqiao Li have contribute equally.

*Correspondence:
Xuetao Pei
peixt@nic.bmi.ac.cn
Yanhua Li
shirlylyh@126.com
Full list of author information is available at the end of the article

Chen *et al. Stem Cell Research & Therapy*   (2024) 15:133

Page 2 of 12

Introduction

In recent years, various tissue-specific organoids have been generated in vitro based on their capacity for stem cell proliferation, differentiation, and self-organization within a three-dimensional (3D) microenvironment [1–3]. Organoid culture techniques have been continuously developed and applied in disease modeling, drug candidate screening, and investigation of pathophysiological mechanisms [4]. Given the important potential applications of hematopoietic organoids and organ-on-a-chip systems, several laboratories are dedicated to the manufacturing and assessment of their utility in disease modeling, particularly for conditions such as radiation injury and bone marrow (BM) fibrosis [1, 5]. Nevertheless, establishing a reliable culture technique for hematopoietic organoids remains a formidable challenge owing to the intrinsic complexity of hematopoietic tissues.

Hematopoietic stem cells (HSCs), situated at the apex of the hematopoietic system, have the ability to self-renew and differentiate into multilineage blood cells [6], which are critical seed cells for manufacturing of hematopoietic organoids. However, enriching rare adult HSCs and their progenitor cells (HSPCs) in the BM is a significant challenge. The limited number and expansion capacity of HSPCs from a single cord blood sample also impede the development of large numbers of homogeneous hematopoietic organoids. Human pluripotent stem cells (hPSCs), including induced pluripotent stem cells (iPSCs) and human embryonic stem cells (hESCs), have indefinite capacity for self-renewal and the potential to differentiate into HSPCs [7]. hPSCs-derived HSPCs may be ideal seed cells for generating human hematopoietic organoids [8–10]. In vivo, adult HSPCs inhabit a specialized BM niche comprising a variety of stromal cells, such as mesenchymal cells, endothelial cells, osteocytes, and the extracellular matrix (ECM) [11–13], which collectively provide intricate biochemical and physical cues essential for the regulation and maintenance of HSPC function. To construct a biomimetic bone marrow microenvironment in vitro, multiple cell lines, such as bone marrow stromal cells (HS-5), human umbilical vein endothelial cells (HUVECs) or human umbilical artery endothelial cells (HUAECs), and osteoblasts (hFOB 1.19) have been used in culture systems to support HSPC survival, proliferation, and differentiation [14–17]. The 3D scaffold is another important factor in mimicking the hematopoietic microenvironment. In recent years, gelatin-methacryloyl (GelMA) hydrogels have become an alternative scaffold material for constructing a 3D microenvironment or acting as a cell-laden bioprinting bio ink, owing to their good biocompatibility and tunable physicochemical properties [18]. It is important to investigate whether human hematopoietic organoids can be manufactured with GelMA and multiple niche-related cells, and whether these organoids can be used as a disease model, such as a radiation-injured model, to evaluate drug response.

In this study, we proposed a method for constructing hematopoietic organoids using a GelMA-based 3D culture system with HSPCs derived from hESCs. To better mimic the bone marrow microenvironment, we incorporated niche-related cells such as HS-5 cells, HUAECs, and hFOB 1.19 cells into the GelMA. Our data suggests that the presence of these niche cells creates a more favorable microenvironment for the formation of hematopoietic organoids. Furthermore, our findings demonstrate that these hematopoietic organoids display radiation-induced injury to hematopoietic cells and show responsiveness to granulocyte colony-stimulating factor (G-CSF). This study contributes to the advancement of standardized and scalable production methods for hematopoietic organoids, which can greatly facilitate their utilization in disease modeling and drug testing.

Materials and methods

hESC culture and differentiation

H9 human embryonic stem cells (H9-hESCs; WiCell Research Institute) were maintained on Matrigel (CORNING, Corning, NY, USA) and cultured in mTeSR1 medium (STEMCELL Technologies, Vancouver, Canada). The medium was refreshed daily, and the cells were passaged at 4–6 day intervals using TrypLE Select (Thermo Fisher Scientific, Waltham, MA, USA). On Day 0, hESCs were plated at a density of 1×10^4 cells/cm^2 and cultured for 24 h in the mTeSR medium. The following day (day 1), the medium was replaced with BEL medium supplemented with 25 ng/ml bFGF (PeproTech, Rocky Hill, NJ, USA), 25 ng/ml BMP4, 25 ng/ml Activin A (both from R&D Systems, Minneapolis, MN, USA), and 2 μM CHIR99021 (Selleck, Houston, TX, USA), and the cells were cultured for an additional 48 h (Stage I). Afterwards, cells were rinsed with phosphate-buffered saline (PBS) and transitioned to Stage II BEL medium, enhanced with 50 ng/ml VEGF (R&D Systems), 20 ng/ml bFGF (Selleck), and 2 μM SB431542 (Selleck), and incubated for 72 h. After incubation, the cells were dissociated into single-cell suspensions. CD34$^+$ cells were then isolated by positive selection using a MACS CD34 MicroBead Kit (Miltenyi Biotec, Gladbach Bergisch, Germany) [19–21]. Isolated CD34$^+$ cells were then resuspended in BEL medium containing 50 ng/mL SCF (PeproTech), 20 ng/mL TPO (PeproTech), 20 ng/mL IL-3 (PeproTech), 20 ng/mL Flt3L (PeproTech), 20 ng/ml VEGF, 10 ng/mL bFGF, and 5 μM SB431542. Cells were seeded at a density of 2×10^4 cells/cm^2 in Matrigel-coated culture dishes and

cultured for 96 h. At the end of this period, the supernatants were harvested, and $CD34^+$ hematopoietic progenitor cells were further purified using the MACS CD34 MicroBead Kit. The BEL medium composition followed a published reference (see Additional file 2: Table S1) [22], and the main reagents utilized for hESCs maintenance and differentiation are outlined in Additional file 4: Table S3 and Additional file 5: Table S4.

Stromal cell culture

HS-5 cells (ATCC) were cultured in Dulbecco's Modified Eagle Medium (DMEM) supplemented with 10% fetal bovine serum (FBS) (both from Thermo Fisher Scientific) at 37 °C. The medium was refreshed every two days, and the cells were passaged every 3–4 days using trypsin–EDTA [23].

HUAECs were cultured in EGM-2 medium (Lonza, Basel, Switzerland) at 37 °C [16]. The medium was refreshed every two days, and the cells were passaged every 3–4 days using TrypLE Select.

hFOB 1.19 cell line (Cell Bank/Stem Cell Bank of the Chinese Academy of Sciences) was cultured in DMEM/F12 medium supplemented with 10% FBS and 0.3 mg/ml G418 (Thermo Fisher Scientific) at 33.5°. The medium was refreshed every two days, and the cells were passaged every 4–5 days using TrypLE Select [14].

Preparation and cell culture of GelMA hydrogel

GelMA (EFL, Suzhou, China) was solubilized in a PBS solution containing 0.25% (w/v) lithium phenyl-2,4,6-trimethylbenzoylphosphinate (LAP; EFL) to attain a final GelMA concentration of 10% (w/v). The mixture was heated to 85 °C in a water bath shielded from light for 45 min and subsequently sterile-filtered.

For co-culture experiments, $CD34^+$ cells were labeled with 2 μM carboxyfluorescein succinimidyl ester (CFSE) dye (Thermo Fisher Scientific) [20].

HS-5 cells, HUAECs, and hFOB 1.19 cells and hESCs-derived $CD34^+$ cells were seeded into GelMA hydrogel at a ratio of 1:1:1:3 to achieve a final density of 1×10^6 cells/mL for $CD34^+$ cells. The GelMA and cell mixture was then deposited in ultra-low attachment 24-well plates and polymerized using UV light for 51 s. In the GelMA hydrogel group, $CD34^+$ cells pre-labeled with CFSE dye were encapsulated in GelMA at a density of 1×10^6 cells/mL. Both groups were cultured in a 1:1 mixture of BEL and EGM-2 media, respectively. The BEL medium was supplemented with 50 ng/mL SCF, 20 ng/mL TPO, 20 ng/mL IL-3, 20 ng/mL Flt3L, 5 ng/mL bFGF, and 5 μM SB431542. All cell cultures were maintained at 37 °C with 5% CO_2, with media refreshment every 2 days.

Suspension culture of HSPCs

For the suspension culture of $CD34^+$ cells, an equal number of CFSE-stained $CD34^+$ cells were plated in 6-well plates, corresponding to the amounts utilized in both the GelMA hydrogel co-culture and isolated $CD34^+$ cell cultures. The cells were subsequently incubated at 37 °C with 5% CO_2 in a mixed medium composed of BEL and EGM-2 media at a 1:1 ratio. The BEL medium was fortified with 50 ng/mL SCF, 20 ng/mL TPO, 20 ng/mL IL-3, 20 ng/mL Flt3L, 5 ng/mL bFGF, and 5 μM SB431542. Throughout the cultivation period, the medium was refreshed or replaced daily.

Flow cytometry analysis

For the analysis of cell surface antigens, cells were harvested using GelMA Lysis Buffer (EFL), rinsed once with PBS, and subsequently incubated with specific antibodies diluted in PBS for 30 min at 4 °C in darkness. Following staining, the cells were examined using a BD FACS Aria II flow cytometer (BD Biosciences, Franklin Lakes, NJ, USA), and the data were processed using FlowJo software (TreeStar, Ashland, OR, USA) [24, 25]. The antibody details are provided in Additional file 2: Table S2.

Immunofluorescence assay

For the 3D cell-staining experiment, GelMA laden with cells was fixed with 4% paraformaldehyde at room temperature for one hour. Subsequently, the samples were permeabilized with 0.3% Triton X-100 in PBS for 30 min and blocked with 10% donkey serum in PBS for two hours. Primary antibodies were applied in 10% donkey serum and incubated overnight at 4 °C, washed three times for 1 h each. The secondary antibodies were incubated overnight at room temperature and subjected to the same washing steps. The nuclei were stained with 10 μg/ml DAPI for 15 min. Fluorescence microscopy images were captured using a confocal microscope (PerkinElmer, Waltham, MA, USA) [24, 26]. Detailed information on the antibodies used is provided in Additional file 2: Table S2.

ELISA assay

For the ELISA assay, cells were collected using GelMA Lysis Buffer. The levels of CXCL12 in the cells were detected by using Human CXCL12 ELISA Kit (BOSTER, Wuhan, China) according to the manufacturer's instructions.

Colony-forming unit assay

For the hematopoietic colony-forming unit (CFU) assay, cells were collected using GelMA Lysis Buffer

Chen *et al. Stem Cell Research & Therapy*   (2024) 15:133

Page 4 of 12

and fixed at a density of 5×10^5 cells/mL. A 100 µL cell suspension was then combined with 0.5 mL of H4636 hematopoietic colony culture medium (STEMCELL Technologies), thoroughly mixed, and dispensed into ultra-low attachment 24-well plates. After 14 days of incubation, colonies were enumerated and classified based on morphology into erythroid (BFU-E, burst-forming unit-erythroid), myeloid (CFU-GM, colony-forming unit-granulocyte, monocyte), or mixed lineage (CFU-GEMM, colony-forming unit granulocytes, erythrocytes, monocytes, and megakaryocytes) categories [21].

G-CSF administration after radiation
Immediately after exposure to 2 or 4 Gy radiation, the medium was replaced with a mixture of BEL and EGM-2 (as previously described) supplemented with 100 ng/mL G-CSF. The culture was maintained by daily replacement with fresh medium containing 100 ng/mL G-CSF.

Statistical analysis
Statistical analyses were conducted using GraphPad Prism 8 software (GraphPad, Inc., La Jolla, CA, USA). Data are presented as means ± SD. The statistical significance of the differences was assessed using an unpaired two-tailed Student's t-test, one-way ANOVA, or two-way ANOVA, as appropriate. Statistical significance was considered at $p < 0.05$, denoted as *$p < 0.05$, **$p < 0.01$ and ***$p < 0.001$.

Result
GelMA hydrogel is capable of maintaining undifferentiated state of hESCs-derived HSPCs
hESCs are ideal seed cells for generation of large numbers of HSPCs for hematopoietic organoid construction. Thus, we first opted for an adherent induction protocol to produce mesodermal progenitors, hemogenic endothelial cells, and HSPCs from hESCs within a 9-day induction period (Fig. 1a). Cultured hESCs were orderly exposed to a three-stage differentiation culture medium, resulting in the gradual emergence of semi-adherent and adherent hematopoietic-like cells (Fig. 1b, c). Subsequently, populations of hematopoietic-like cells were selectively enriched using CD34+ immunomagnetic bead sorting [21]. Flow cytometry analysis revealed high expression levels of CD43, CD34, and CD45 in these cells, with CD43+CD34+ cells comprising approximately 93.70% and CD34+CD45+ cells constituting approximately 38.50% of the population (Fig. 1d). Additionally, the presence of CD34, CD43, and CD45 proteins was confirmed by immunofluorescence staining (Fig. 1e), providing further evidence of the successful collection of HSPCs from hESCs.

To construct hematopoietic organoids, GelMA hydrogel was selected as the 3D scaffold into which hESCs-derived CD34+ HSPCs were seeded (Fig. 1f) [26–29]. Interestingly, we found that the CD34+ cell percentage was significantly higher in the 3D GelMA culture microenvironment than in the two-dimensional (2D) liquid culture condition (Fig. 1g). Colony-forming unit (CFU) assay results revealed that the total colony count markedly increased in the 3D GelMA culture group after a 7-day culture (Fig. 1h). These results suggested that the GelMA hydrogel more effectively maintained the proportion of hESCs-derived HSPCs in vitro (Fig. 1g). Furthermore, we examined the cell cycles of CD34+ and CD45+ cells under 2D and 3D GelMA culture conditions. We found that hESCs-derived CD34+ and CD45+ hematopoietic cells presented lower cell percentages in the G2/M/S phase and higher percentages in the G0/G1 phase when cultured in 3D conditions (Fig. 1i). Additionally, lower levels of ROS were detected in hESCs-derived CD34+ HSPCs in the 3D GelMA culture (Fig. 1j), suggesting that the GelMA hydrogel may maintain the undifferentiated state of HSPCs by reducing ROS levels and maintaining more cells in a resting state. These indicate that the GelMA hydrogel was favorable for maintaining the undifferentiated state of hESCs-derived CD34+ HSPCs in vitro.

Establishment of human hematopoietic organoids in GelMA hydrogel with niche-related cells
To accurately simulate the complicated BM hematopoietic microenvironment in GelMA in vitro, the GelMA hydrogel was supplemented with several types of BM niche-related cells, including HS-5 cells, HUAECs, and hFOB1.19 cells, to support hematopoietic cell survival, proliferation, and differentiation [14–17]. HS-5 cells, HUAECs, and hFOB 1.19 cells and hESCs-derived CD34+ cells were seeded into GelMA hydrogel at a ratio of 1:1:1:3 (Fig. 2a). Notably, hESCs-derived CD45+ cells exhibited adherent growth on hematopoietic niche cells (+Niche cell group), whereas CD45+ cells on GelMA without niche cells (− Niche cell group) showed single- or spheroid-like growth after 7 days of culture (Fig. 2b). Moreover, HS-5 cells, HUAECs, and hFOB1.19 cells normally expressed characteristic proteins in this culture environment (Fig. 2c). Additionally, although there was no significant difference in the proportion of CD34+CD45+ HSPCs between the two groups, the presence of niche cells in GelMA resulted in a higher number of CD34+CD45+ HSPCs than in their absence (Fig. 2d, e), indicating that niche cells support the proliferation of CD34+CD45+ HSPCs. The CFU assay results showed that the total number of colonies significantly increased in the +Niche cell group after seven days of culture
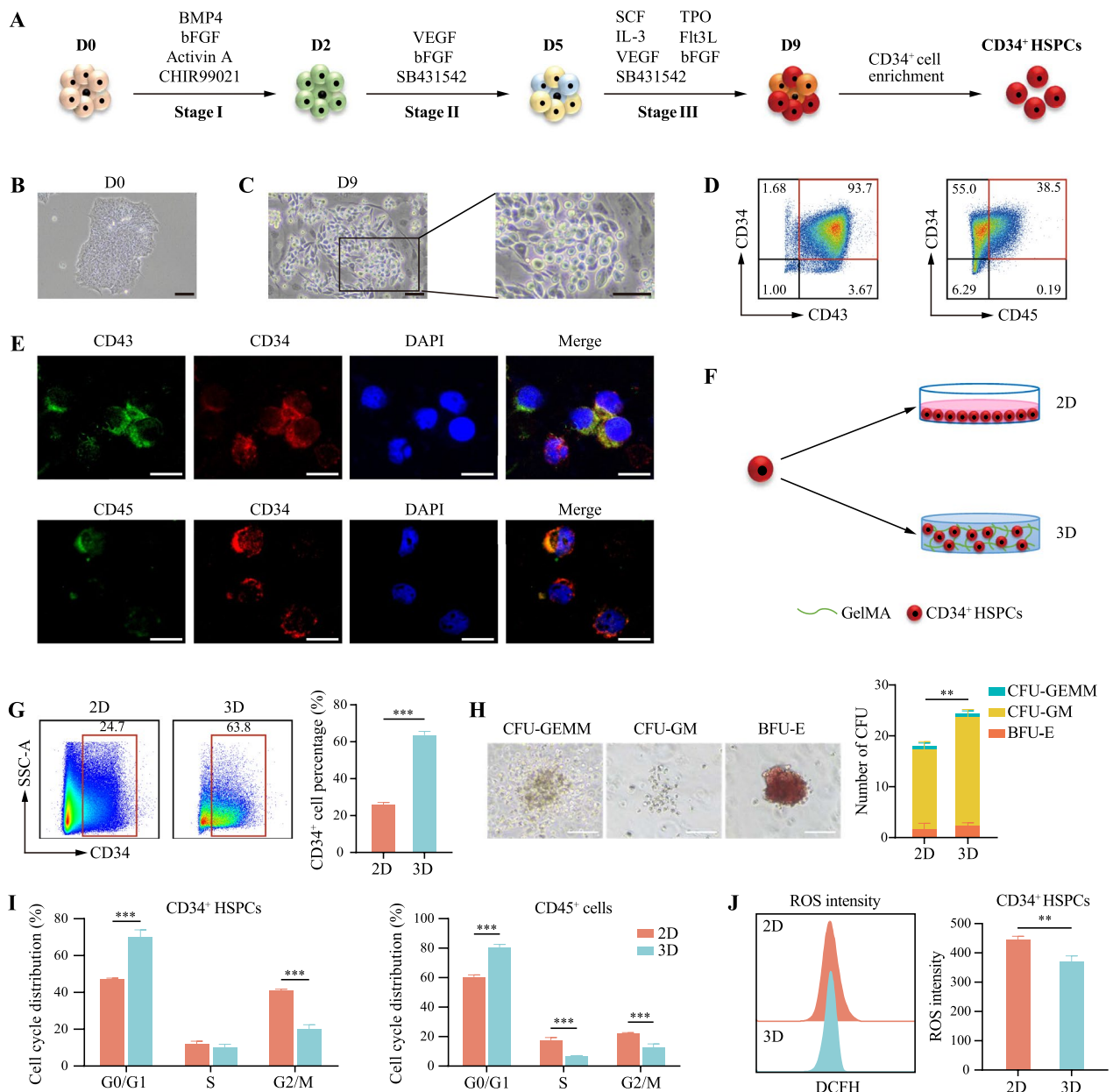
Fig. 1 Establishment of a hESC-to-HSPC differentiation system and the application of GelMA in vitro culture. **a** Schematic diagram of the differentiation from hESCs to HSPCs. **b** Representative morphology of hESCs-H9 cells (scale bar, 100 µm). **c** Representative morphologies of HSPCs induced from hESCs-H9 cells (scale bar, 50 µm). **d** Flow cytometry analysis of the expression of CD34, CD43, and CD45 on the induced HSPCs. **e** Immunofluorescence staining for the detection of CD34, CD43, and CD45 expression on the induced HSPCs (scale bar, 20 µm). **f** Schematic diagram of 2D and 3D-GelMA culture. **g** Percentage of CD34$^+$ cells on day 7 for each condition. Results are presented as the mean ± SD from three independent experiments. Unpaired Student's *t*-test, ***$p < 0.001$. **h** Representative morphologies of different colony types (CFU-GEMM, CFU-GM and BFU-E) and total number of colonies under different culture conditions (scale bar, 100 µm). Results are presented as the mean ± SD from three independent experiments. Unpaired Student's *t*-test, **$p < 0.01$. **i** Percentage of CD34$^+$ and CD45$^+$ cells in G0/G1, S and G2/M phase of the cell cycle for each condition after 7-day culture. Results are presented as the mean ± SD from three independent experiments. Two-way ANOVA, ***$p < 0.001$. **j** Intracellular ROS levels within CD34$^+$ cells were determined utilizing DCFH assay via flow cytometry. Results are presented as the mean ± SD from three independent experiments. Unpaired Student's *t*-test, **$p < 0.01$

Chen *et al. Stem Cell Research & Therapy*   (2024) 15:133
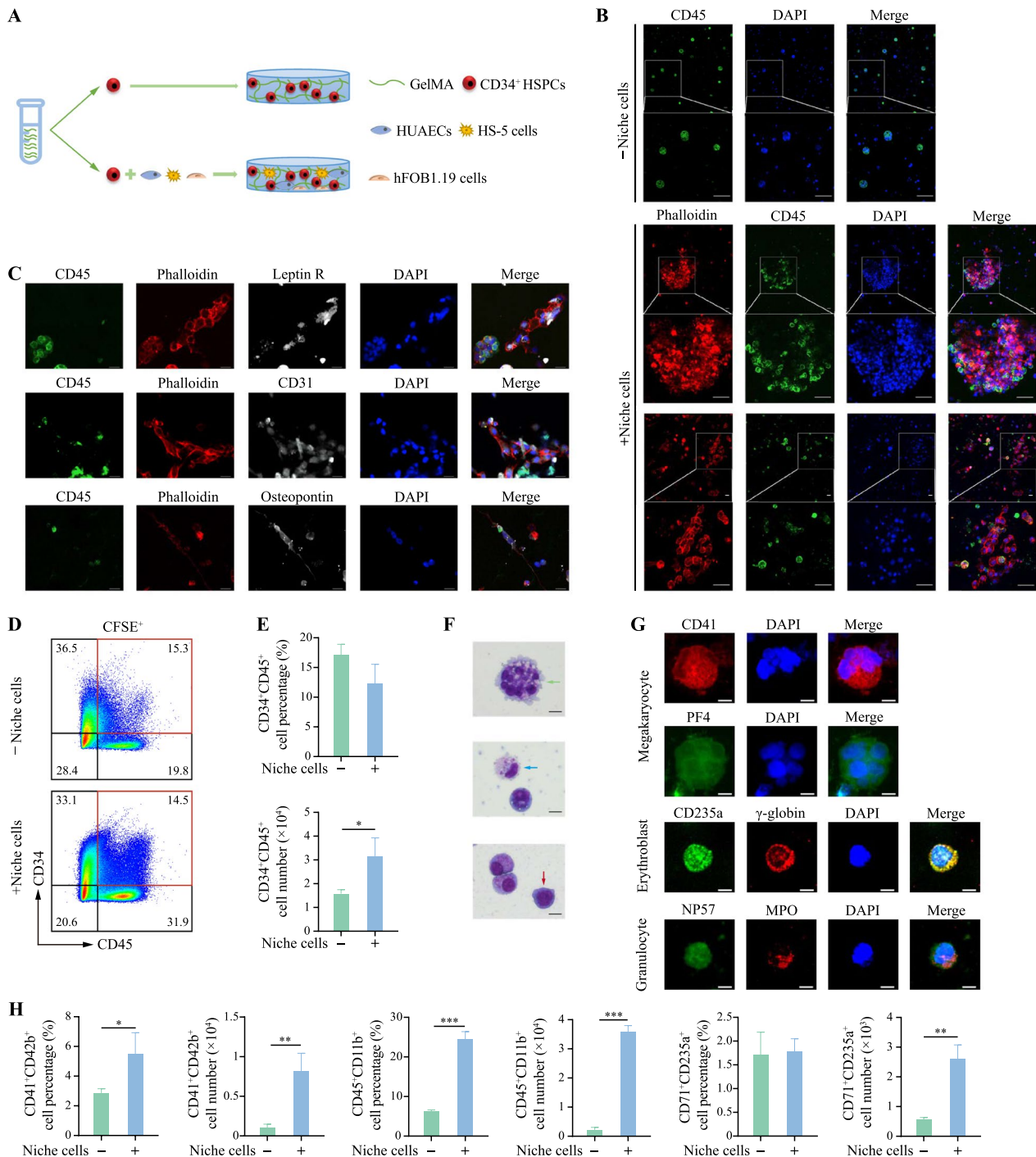
Page 6 of 12

Fig. 2 Construction of the in vitro hematopoietic organoids. **a** Schematic diagram of the construction of the hematopoietic organoids. **b** Immunofluorescence images of cells in GelMA under different conditions (scale bar, 50 μm). **c** Various niche cell-specific protein immunofluorescence staining in GelMA with niche cell groups (scale bar, 20 μm). **d** Flow cytometry analysis of CD34 and CD45 expression in cells for each condition. **e** Percentage and number of CD34$^+$CD45$^+$ cells on day 7 for each condition. Results are presented as the mean ± SD from three independent experiments. Unpaired Student's t-test, *$p < 0.05$. **f** Giemsa staining of megakaryocytes, promyelocytes, and erythroblasts from GelMA with niche cells group on day 7 (green: megakaryocytes; blue: promyelocytes; red: erythroblasts. scale bar, 10 μm). **g** Immunofluorescence staining showed the expression of specific proteins associated with megakaryocytes (CD41 and PF4), erythroid cells (CD235a and γ-globin), and granulocytes (NP57 and MPO) when co-cultured with niche cells. Scale bars, 10 μm. **h** Percentage and number of CD41$^+$CD42b$^+$, CD45$^+$CD11b$^+$ and CD71$^+$CD235a$^+$ cells on day 7 for each condition. Results are presented as the mean ± SD from three independent experiments. Unpaired Student's t-test, *$p < 0.05$; **$p < 0.01$; ***$p < 0.001$

(Additional file 6: Supplementary Fig. 1). Of note, Wright-Giemsa staining demonstrated the presence of mega-karyocytes, promyelocytes and erythroblasts in these organoids (Fig. 2f). Consistently, immunostaining results showed large polyploid megakaryocytes with PF4 protein expression, granulocytes with NP57 and MPO expression, and CD235$^+$ erythroid cells with γ-globin protein expression (Fig. 2g). Compared to the -Niche cell group, the + Niche cell group exhibited a higher quantity of meg-akaryocytic (CD41$^+$CD42b$^+$), myeloid (CD45$^+$CD11b$^+$), and erythroid (CD71$^+$CD235a$^+$) cells (Fig. 2h). These results indicate that the integration of niche cells into GelMA creates a more conducive microenvironment for the formation of hematopoietic organoids, thereby enhancing the proliferation and multilineage differentiation capabilities of hESCs-derived HSPCs.

The hematopoietic organoids exhibit radiation-induced hematopoietic cell injury effect

To assess the impact of niche cells in GelMA on HSPCs in radiation damage, organoids were exposed to 4 Gy doses of ionizing radiation (IR) in GelMA with and without niche cells (Fig. 3a). Higher protein concentration of CXCL12 is found in the + Niche cell group compared to those in the -Niche cell group, suggesting that niche cells may interact with hematopoietic cells through chemokine/chemokine receptor axis (Fig. 3b). Previous studies have reported an increase in CXCL12 levels in
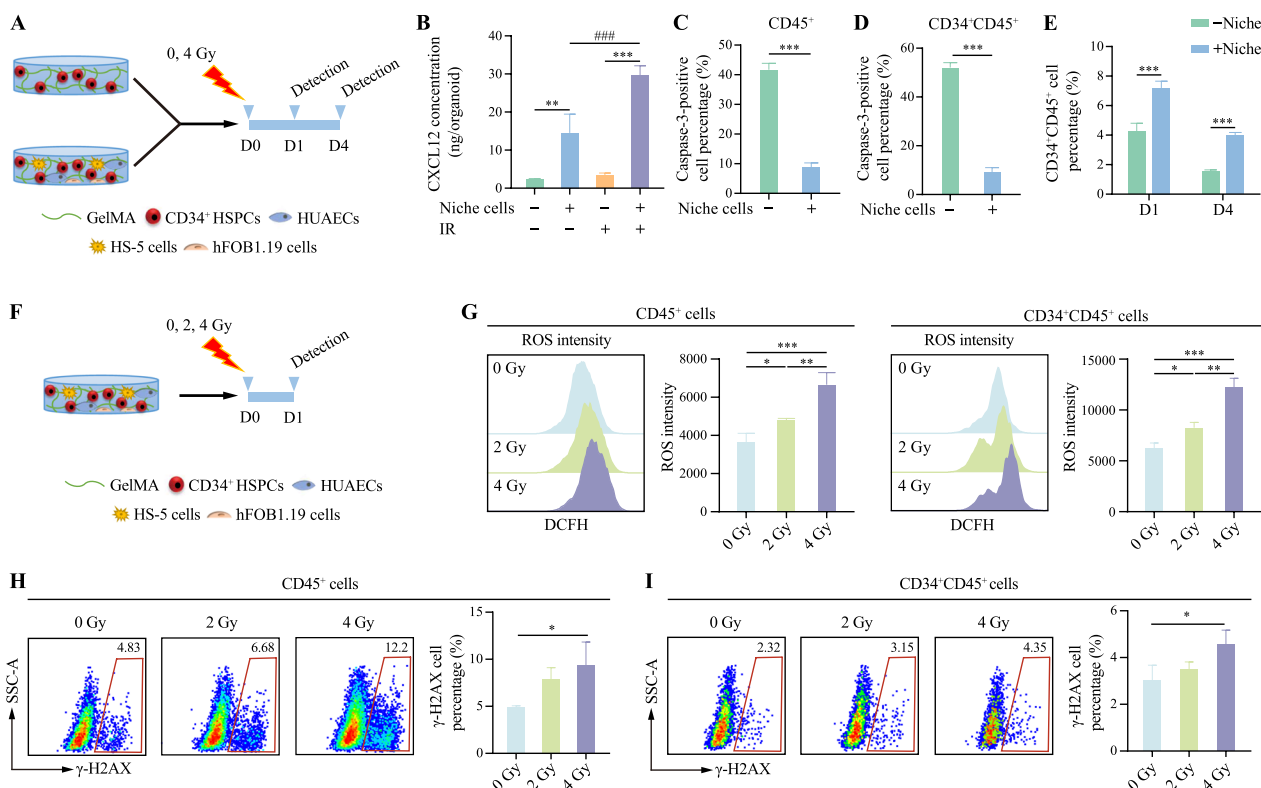

Fig. 3 Construction of the in vitro radiation injury model based on the hematopoietic organoids. **a** Schematic diagram demonstrates the organoids from -Niche cell and + Niche cell groups received radiation at 0 or 4 Gy. **b** Comparative analysis of CXCL12 concentration in the two groups under different conditions one day after radiation exposure. Results are presented as the mean ± SD from three independent experiments. One-way ANOVA, **$p < 0.01$; ***$p < 0.001$;###$p < 0.001$. **c** Flow cytometry analysis of the percentage of caspase-3-positive cells in CD45$^+$ cell population from the two groups one day after radiation exposure. Results are presented as the mean ± SD from three independent experiments. One-way ANOVA, ***$p < 0.001$. **d** Flow cytometry analysis of the percentage of caspase-3-positive cells in CD34$^+$CD45$^+$ cell population from the two groups one day after radiation exposure. Results are presented as the mean ± SD from three independent experiments. One-way ANOVA, ***$p < 0.001$. **e** Percentage of CD34$^+$CD45$^+$ cells on the first and fourth day after 4 Gy irradiation. Results are presented as the mean ± SD from three independent experiments. One-way ANOVA, ***$p < 0.001$. **f** Schematic diagram of the construction of the radiation injury model. **g** ROS levels in CD45$^+$ and CD34$^+$CD45$^+$ cells under different radiation doses. Results are presented as the mean ± SD from three independent experiments. One-way ANOVA, *$p < 0.05$; **$p < 0.01$; ***$p < 0.001$. **h** γ-H2AX expression levels in CD45$^+$ cells under different radiation doses. Results are presented as the mean ± SD from three independent experiments. One-way ANOVA, *$p < 0.05$. **I.** γ-H2AX expression levels in CD34$^+$CD45$^+$ cells under different radiation doses. Results are presented as the mean ± SD from three independent experiments. One-way ANOVA, *$p < 0.05$

Chen *et al. Stem Cell Research & Therapy*   (2024) 15:133

Page 8 of 12

the BM niche after radiation exposure [30, 31]. We further employed ELISA to measure CXCL12 levels in the organoids before and after radiation. Notably, radiation significantly increased CXCL12 protein concentration in the + Niche cell group (Fig. 3b), a similar response with in vivo bone marrow tissue before and after irradiation. However, the organoids in −Niche cell group exhibited no obvious alteration on CXCL12 protein concentration between non-irradiated and irradiated conditions (Fig. 3b). Furthermore, compared to the -Niche cell group, the + Niche cell group showed a notable reduction in the percentage of caspase-3-positive cells at day 1 post-radiation and significant increases in $CD34^+CD45^+$ cell percentages at day 1 and day 4 after radiation damage (Fig. 3c–e). These findings reflect the potential protective effects of niche cells on HSPCs during the radiation injury process.

To further evaluate whether human hematopoietic organoids have different responses at different doses of IR, the organoids formed in GelMA with niche cells were exposed to IR at doses of 2 and 4 Gy (Fig. 3f). Notably, we found that IR induced dose-dependent increases in ROS-positive cell percentages within the $CD45^+$ cell population at day 1 after exposure (Additional file 7: Supplementary Fig. 2). Concurrently, flow cytometry analysis results further demonstrated that IR induced a progressive increase in oxidative stress damage in $CD45^+$ and $CD34^+CD45^+$ cells, as evidenced by elevated ROS

levels with increased radiation doses (Fig. 3g). Moreover, exposure to a 4 Gy dose of IR significantly augmented the proportion of γ-H2AX-positive cells in $CD45^+$ and $CD34^+CD45^+$ populations (Fig. 3h, i), indicating that the hematopoietic organoid can be injured at DNA levels after high dose of radiation.

Subsequently, we evaluated apoptosis in hematopoietic organoids one day after irradiation exposure by assessing caspase-3 expression (Fig. 4a). Remarkably, radiation with 2 and 4 Gy significantly elevated the percentage of caspase-3-positive cells in $CD45^+$ cells by 1.22- and 2.07-fold, respectively, compared to that in the non-irradiated group (Fig. 4b). Additionally, in $CD34^+CD45^+$ cells, the percentage of caspase-3-positive cells increased by 0.07- and 0.94-fold, respectively (Fig. 4b). The overall cell count on the fourth day post-irradiation showed that compared with the non-irradiated group, the cell count decreased by approximately 33% and 39% after 2 Gy and 4 Gy irradiation, respectively, aligning with the radiation sensitivity observed in human studies [32] (Additional file 4: Supplementary Fig. 3). In addition, the numbers of blood cells ($CD45^+$), HSPCs ($CD34^+CD45^+$), myeloid cells ($CD45^+CD11b^+$), and erythrocytes ($CD71^+CD235a^+$) decreased by approximately 68%, 43%, 59%, and 47% respectively after 4 Gy irradiation, showing relatively severe cytotoxic effects (Fig. 4c–e). These findings highlight the susceptibility of hematopoietic organoids to radiation-induced damage.
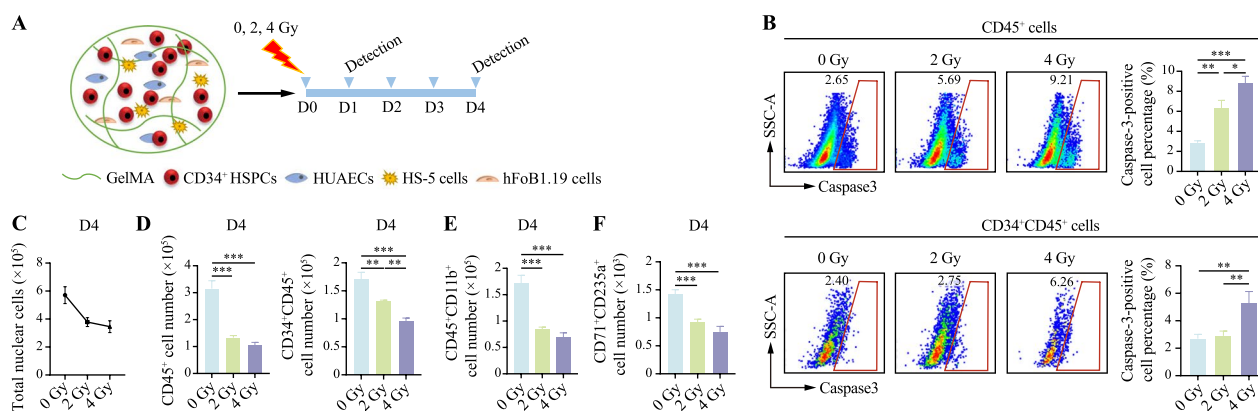

Fig. 4 The hematopoietic organoids exhibit radiation-induced hematopoietic cell injury effect. **a** Schematic diagram of apoptosis detection in the radiation injury model after exposure to different doses on the first and fourth days. **b** Flow cytometry analysis of the percentage of caspase-3-positive cells in $CD45^+$ and $CD34^+CD45^+$ cells under different radiation doses. Results are presented as the mean ± SD from three independent experiments. One-way ANOVA, *$p < 0.05$; **$p < 0.01$; ***$p < 0.001$. **c** Flow cytometry analysis of the total number of nuclear cells under different radiation doses. **d** Flow cytometry analysis of the number of $CD45^+$ and $CD34^+CD45^+$ cells under different radiation doses. Results are presented as the mean ± SD from three independent experiments. One-way ANOVA, **$p < 0.01$; ***$p < 0.001$. **e** Flow cytometry analysis of the number of $CD45^+CD11b^+$ cells under different radiation doses. Results are presented as the mean ± SD from three independent experiments. One-way ANOVA, ***$p < 0.001$. **f** Flow cytometry analysis of the number of $CD71^+CD235a^+$ cells under different radiation doses. Results are presented as the mean ± SD from three independent experiments. One-way ANOVA, ***$p < 0.001$

Chen *et al. Stem Cell Research & Therapy*   (2024) 15:133
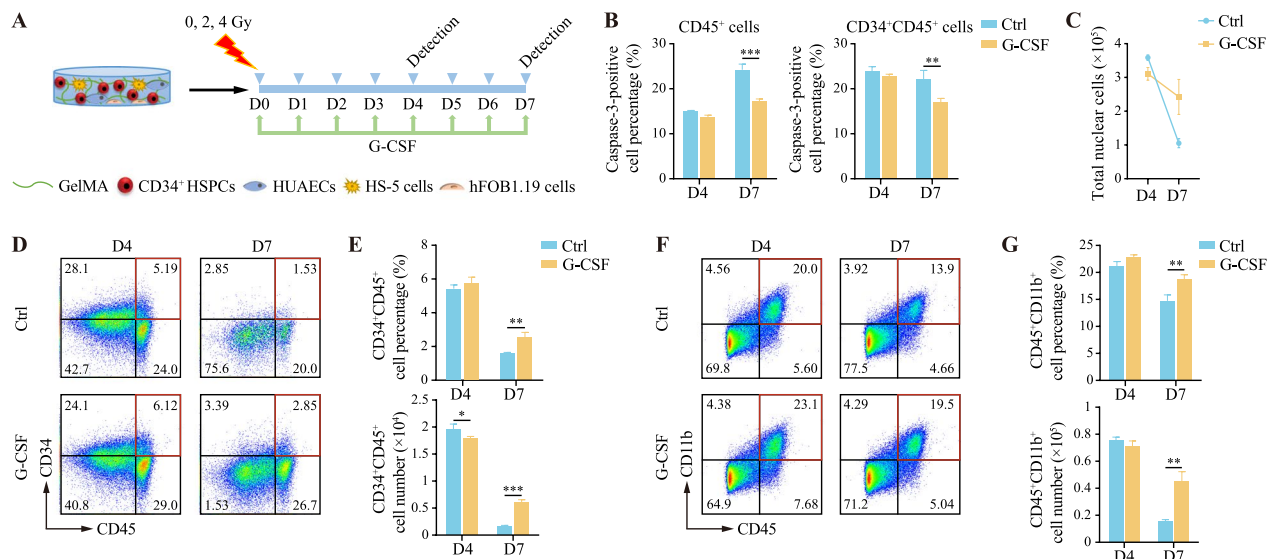
Page 9 of 12

Fig. 5 G-CSF exhibits a radiation-mitigating effect in hematopoietic cells. **a** Schematic diagram for effect of G-CSF on hematopoietic cells after radiation exposure. **b** Flow cytometry analysis of the percentage of caspase-3-positive cells in $CD45^+$ and $CD34^+CD45^+$ cells in the radiation injury model on the fourth and seventh days following the administration of G-CSF after irradiation. Results are presented as the mean ± SD from three independent experiments. Two-way ANOVA, **$p < 0.01$; ***$p < 0.001$. **c** Flow cytometry analysis of the number of total nuclear cells in the radiation injury model on the fourth and seventh days following the administration of G-CSF after radiation. **d–e** Flow cytometry analysis of the percentage and number of $CD34^+CD45^+$ cells in the radiation injury model on the fourth and seventh days following the administration of G-CSF after radiation. Results are presented as the mean ± SD from three independent experiments. Two-way ANOVA, *$p < 0.05$; **$p < 0.01$; ***$p < 0.001$. **f–g** Flow cytometry analysis of the percentage and number of $CD45^+CD11b^+$ myeloid cells in the radiation injury model on the fourth and seventh days following the administration of G-CSF after radiation. Results are presented as the mean ± SD from three independent experiments. Two-way ANOVA, **$p < 0.01$

Hematopoietic organoids post-radiation can be used to evaluate the radiation-mitigating effects of G-CSF

G-CSF is a myeloid growth factor considered as an ideal medication for reducing radiation-induced BM suppression [33]. Following the administration of G-CSF after 4 Gy irradiation in hematopoietic organoids (Fig. 5a), a significant reduction in the percentage of caspase-3-positive cells within both $CD45^+$ and $CD45^+CD34^+$ cells was observed by the seventh day (Fig. 5b). Simultaneously, from the fourth to the seventh day of culture, the cell counts in the G-CSF treated group decreased by approximately 22%, in stark contrast to a 70% reduction in the control group (Fig. 5c). Furthermore, after G-CSF addition, there was a significant increase in the proportion and number of $CD45^+CD34^+$ HSPCs and $CD45^+CD11b^+$ myeloid cells (Fig. 5d–g), which is consistent with previous findings that G-CSF stimulates the proliferation of HSPCs and induces myeloid cell differentiation, thus ameliorating acute damage to the hematopoietic system caused by radiation [34, 35]. These findings demonstrate the effectiveness of G-CSF in safeguarding blood cells after radiation injury, and reflect the utility of hematopoietic organoids in assessing therapeutic strategies for the mitigating and rehabilitation of bone marrow radiation damage.

Discussion

In this study, we aimed to establish hematopoietic organoids using hESCs-derived HSPCs, niche-related cells, and a GelMA hydrogel and to evaluate their utility for modeling hematopoietic injury and regeneration. Although various tissue-specific organoids have been generated and applied in the biomedical field, establishing human hematopoietic organoids or BM on-a-chip models remains a significant challenge because of the inherent complexity of BM tissues. HSPCs are the key seed cells in the production of hematopoietic organoids. However, it is difficult to obtain rare HSPCs from mobilized peripheral blood, BM, or a single unit of cord blood. hPSCs, such as hESCs, are ideal seed cells for obtaining large numbers of HSPCs and for scalable manufacturing of human hematopoietic or BM organoids. Accumulating evidence demonstrates that hESCs can differentiate into HSPCs and multilineage blood cells [36, 37]. Therefore, we used a stepwise induction protocol to generate human $CD34^+$ HSPCs from hESCs.

The manufacture of organoids often requires the use of Matrigel or hydrogels to provide a 3D biomimetic microenvironment [38, 39]. Among various hydrogels, GelMA has been widely applied in 3D cell culture and has demonstrated its capacity to effectively simulate

the biophysical properties of the ECM and promote cell adhesion and growth [40]. GelMA possesses an arginine-glycine-aspartic acid (RGD) sequence and a target sequence for matrix metalloproteinases (MMPs) and can be modified according to different requirements [41]. In recent years, GelMA and other types of hydrogels have been used to support HSPC growth and expansion, demonstrating the reliability of these hydrogels for 3D hematopoietic organoid modeling. Notably, we found that the GelMA hydrogel as a 3D scaffold could support hESCs-derived HSPC survival and maintain an undifferentiated state. An increasing number of studies have demonstrated that in vitro culture of HSPCs causes non-physiological oxidative stress injury and leads to a decreased self-renewal capacity of HSCs [42, 43]. Notably, our 3D culture system based on the GelMA hydrogel has the advantage of reducing ROS levels in HSPCs, which supports its role in maintaining HSPC function. The maintenance of adult hematopoietic function requires BM niche cells that can regulate self-renewal, proliferation, and differentiation of HSCs [44–47]. Various niche-related cell lines with characteristics of endothelial cells, stromal cells, or osteoblasts have been used to support HSPC function or to construct BM-on-a-chip [14]. Based on the complicated characteristics of the BM niche, we designed and established a hematopoietic organoid model consisting of various niche-related cells and GelMA hydrogel. These cells provide crucial signaling molecules like CXCL12 chemokine, Leptin receptor, and osteopontin, essential for HSC self-renewal, proliferation, and differentiation [48, 49]. Moreover, the evident adherence between the niche and the hematopoietic cells reflect the significance of intercellular interactions. The human hematopoietic organoids that we constructed maintained HSPC function and produced myeloid cells, megakaryocytes, and erythroid cells, indicating that this model can recapitulate normal and injury-conditioned human hematopoiesis in vitro.

The similarity of the cell composition and function of our hematopoietic organoids to human BM prompted us to develop a hematopoietic disease model and assess the drug response. The hematopoietic system is highly sensitive to radiation and other chemical factors. Many laboratories are devoted to screening and developing new drugs to protect the hematopoietic system and mitigate hematopoietic injury. However, the lack of scalable human BM organoid platforms has significantly hampered the study of radiation-stressed hematopoiesis and evaluation of novel therapies. We tested and proved that biomimetic hematopoietic organoids show radiation dose-dependent injury responsiveness in hematopoietic cells as evidenced by increased ROS levels and DNA damage degree in them. Accumulated studies indicated that low levels of ROS are essential for maintaining HSC self-renewal whereas radiation induced high ROS level in BM niche that caused HSPC damage [50]. As ROS are known to be involved in hematopoietic injury [51–53], it would be meaningful to further investigate the dynamic change of ROS in different types of hematopoietic and niche cells in the organoids after radiation.

We further tested the responsiveness of this radiation-injured hematopoietic organoid to G-CSF, an FDA-approved radiation countermeasure. We found that G-CSF reduced hematopoietic cell apoptosis and promoted myeloid cell regeneration in the organoids after 4 Gy radiation, which is consistent with its known functions in vivo [35, 54, 55]. Considering that G-CSF can exacerbate radiation-induced long-term BM injury and induce cell senescence [56, 57], more work needs to be done for us to further evaluate the various roles of G-CSF, including extending the culture period of the hematopoietic organoids after radiation and increasing detection criteria after long-term in vitro culture. Additionally, it is worthy to investigate whether the hematopoietic organoids can be used to screen or test HSPC mobilization or homing agents, such as G-CSF, Me6TREN or TPO [58, 59].

Conclusions

Our data demonstrated that 3D hematopoietic organoids composed of HSPCs, multilineage blood cells, and niche-related cells were successfully constructed in vitro. These organoids retained their capacity for HSPCs proliferation and multi-lineage differentiation in vitro. In addition, hematopoietic organoids can produce an organ-level response to radiation toxicity and successfully recapitulate regenerative responses to the radiation countermeasure drug G-CSF. Our study supports the standard and scalable manufacturing of human hematopoietic organoids for radiation-injured or other hematopoietic disease models and drug screening or testing.

Abbreviations

BM	Bone marrow
IR	Ionizing radiation
2D	Two-dimensional
3D	Three-dimensional
GelMA	Gelatin-methacryloyl
hESCs	Human embryonic stem cells
iPSCs	Induced pluripotent stem cells
hPSCs	Human pluripotent stem cells
ROS	Reactive oxygen species
G-CSF	Granulocyte colony-stimulating factor
HSPC	Hematopoietic stem and progenitor cell
ECM	Extracellular matrix
MA	Methacrylic anhydride
RGD	Arginine-glycine-aspartic acid
MMPs	Matrix metalloproteinases
HS-5	Human bone marrow stromal cell line
HUAECs	Human umbilical artery endothelial cells

Chen *et al. Stem Cell Research & Therapy*   (2024) 15:133

Page 11 of 12

hFOB 1.19	Human fetal bone osteoblast cell line
bFGF	Basic fibroblast growth factor
BMP4	Bone morphogenetic protein 4
VEGF	Vascular endothelial growth factor
SCF	Stem cell factor
TPO	Thrombopoietin
IL	Interleukin
Flt3L	Flt3-Ligand
LAP	Lithium phenyl-2,4,6-trimethylbenzoylphosphinate
CFSE	Carboxyfluorescein diacetate succinimidyl ester
PF4	Platelet factor 4
NP57	Neutrophil elastase
MPO	Myeloperoxidase
CFU	Hematopoietic colony-forming unit
BFU-E	Burst-forming unit-erythroid
CFU-GM	CFU-granulocyte, monocyte
CFU-GEMM	CFU-granulocyte, erythrocyte, monocyte and megakaryocyte

Supplementary Information

The online version contains supplementary material available at https://doi.org/10.1186/s13287-024-03743-y.

Additional file 1: Supplemental methods.

Additional file 2: Table S1. The composition of BEL medium.

Additional file 3: Table S2. Antibodies used in this study.

Additional file 4: Table S3. Medium used in this study.

Additional file 5: Table S4. Reagents used in this study.

Additional file 6: Supplemental Figure 1. Total number of colonies under different culture conditions.

Additional file 7: Supplemental Figure 2. Immunofluorescence staining assessed CD45 and DCFH expression under different radiation doses and quantified DCFH positivity in CD45$^+$ cells (scale bar, 50 μm).

Additional file 8: Supplemental Figure 3. Total number of cells under different radiation doses.

Author contributions
K.C. and Y.L. carried out the majority of the described studies, designed and performed experiments, analyzed data, and prepared the manuscript and figures; X.W., X.T., B.Z., T.F., helped with experiments; L.H. helped with manuscript review; X.P. reviewed the manuscript. Y.L. designed and interpreted all experiments and wrote the manuscript. All authors have read and approved the manuscript.

Availability of data and materials
All data generated or analyzed during this study are included in this published article and its supplementary information files.

Declarations

Ethical approval and consent to participate
Not applicable.

Consent for publication
Not applicable.

Competing interests
The authors declare that they have no competing interests.

Author details
[1]College of Chemistry & Materials Science, Hebei University, Hebei, Baoding 071002, China. [2]Key Laboratory of Medicinal Chemistry and Molecular Diagnosis, Hebei University, Hebei, Baoding 071002, China. [3]Stem Cell and Regenerative Medicine Lab, Beijing Institute of Radiation Medicine, Beijing 100850, China.

References
1. Khan AO, Rodriguez-Romera A, Reyat JS, Olijnik AA, Colombo M, Wang G, et al. Human bone marrow organoids for disease modeling, discovery, and validation of therapeutic targets in hematologic malignancies. Cancer Discov. 2023;13:364–85.
2. Wu F, Wu D, Ren Y, Huang Y, Feng B, Zhao N, et al. Generation of hepatobiliary organoids from human induced pluripotent stem cells. J Hepatol. 2019;70:1145–58.
3. Tian CM, Yang MF, Xu HM, Zhu MZ, Yue NN, Zhang Y, et al. Stem cell-derived intestinal organoids: a novel modality for IBD. Cell Death Discov. 2023;9:255.
4. Zhao Z, Chen X, Dowbaj AM, Sljukic A, Bratlie K, Lin L, et al. Organoids. Nat Rev Methods Primers. 2022;2:94.
5. Chou DB, Frismantas V, Milton Y, David R, Pop-Damkov P, Ferguson D, et al. On-chip recapitulation of clinical bone marrow toxicities and patient-specific pathophysiology. Nat Biomed Eng. 2020;4:394–406.
6. Cullen SM, Mayle A, Rossi L, Goodell MA. Hematopoietic stem cell development: an epigenetic journey. Curr Top Dev Biol. 2014;107:39–75.
7. Yang S, Cho Y, Jang J. Single cell heterogeneity in human pluripotent stem cells. BMB Rep. 2021;54:505–15.
8. Motazedian A, Bruveris FF, Kumar SV, Schiesser JV, Chen T, Ng ES, et al. Multipotent RAG1+ progenitors emerge directly from haemogenic endothelium in human pluripotent stem cell-derived haematopoietic organoids. Nat Cell Biol. 2020;22:60–73.
9. Lancaster MA, Knoblich JA. Organogenesis in a dish: modeling development and disease using organoid technologies. Science (N Y N Y). 2014;345:1247125.
10. Gjorevski N, Nikolaev M, Brown TE, Mitrofanova O, Brandenberg N, DelRio FW, et al. Tissue geometry drives deterministic organoid patterning. Science (N Y N Y). 2022;375:eaaw9021.
11. Bello AB, Park H, Lee SH. Current approaches in biomaterial-based hematopoietic stem cell niches. Acta Biomater. 2018;72:1–15.
12. Boulais PE, Frenette PS. Making sense of hematopoietic stem cell niches. Blood. 2015;125:2621–9.
13. Cuddihy MJ, Wang Y, Machi C, Bahng JH, Kotov NA. Replication of bone marrow differentiation niche: comparative evaluation of different three-dimensional matrices. Small. 2013;9:1008–15.
14. Glaser DE, Curtis MB, Sariano PA, Rollins ZA, Shergill BS, Anand A, et al. Organ-on-a-chip model of vascularized human bone marrow niches. Biomaterials. 2022;280:121245.
15. Nelson MR, Ghoshal D, Mejías JC, Rubio DF, Keith E, Roy K. A multi-niche microvascularized human bone marrow (hBM) on-a-chip elucidates key roles of the endosteal niche in hBM physiology. Biomaterials. 2021;270:120683.
16. Li H, Pei H, Wang S, Zhang B, Fan Z, Liu Y, et al. Arterial endothelium creates a permissive niche for expansion of human cord blood hematopoietic stem and progenitor cells. Stem Cell Res Ther. 2020;11:358.
17. Braham MVJ, Li Yim ASP, Garcia Mateos J, Minnema MC, Dhert WJA, Öner FC, et al. A human hematopoietic niche model supporting hematopoietic stem and progenitor cells in vitro. Adv Healthc Mater. 2019;8:1801444.
18. He J, Sun Y, Gao Q, He C, Yao K, Wang T, et al. Gelatin methacryloyl hydrogel, from standardization, performance, to biomedical application. Adv Healthc Mater. 2023;12:e2300395.
19. Rafat A, Dizaji Asl K, Mazloumi Z, Movassaghpour AA, Talebi M, Shanehbandi D, et al. Telomerase inhibition on acute myeloid leukemia stem cell induced apoptosis with both intrinsic and extrinsic pathways. Life Sci. 2022;295:120402.

Chen *et al. Stem Cell Research & Therapy*   (2024) 15:133

Page 12 of 12

20. Jiang J, Qin J, Li J, Lin X, Zhang B, Fan Z, et al. Ricolinostat promotes the generation of megakaryocyte progenitors from human hematopoietic stem and progenitor cells. Stem Cell Res Ther. 2022;13:54.

21. Wu X, Zhang B, Chen K, Zhao J, Li Y, Li J, et al. Baffled-flow culture system enables the mass production of megakaryocytes from human embryonic stem cells by enhancing mitochondrial function. Cell Prolif. 2023;56:e13484.

22. Zhang B, Wu X, Zi G, He L, Wang S, Chen L, et al. Large-scale generation of megakaryocytes from human embryonic stem cells using transgene-free and stepwise defined suspension culture conditions. Cell Prolif. 2021;54:e13002.

23. Osawa T, Wang W, Dai J, Keller ET. Macrofluidic recirculating model of skeletal metastasis. Sci Rep. 2019;9:14979.

24. Fathi E, Mesbah-Namin SA, Vietor I, Farahzadi R. Mesenchymal stem cells cause induction of granulocyte differentiation of rat bone marrow C-kit(+) hematopoietic stem cells through JAK3/STAT3, ERK, and PI3K signaling pathways. Iran J Basic Med Sci. 2022;25:1222–7.

25. Qin J, Zhang J, Jiang J, Zhang B, Li J, Lin X, et al. Direct chemical reprogramming of human cord blood erythroblasts to induced megakaryocytes that produce platelets. Cell Stem Cell. 2022;29:1229-45.e7.

26. Zhang X, Cao D, Xu L, Xu Y, Gao Z, Pan Y, et al. Harnessing matrix stiffness to engineer a bone marrow niche for hematopoietic stem cell rejuvenation. Cell Stem Cell. 2023;30:378-95.e8.

27. Sun M, Sun X, Wang Z, Guo S, Yu G, Yang H. Synthesis and properties of gelatin methacryloyl (GelMA) hydrogels and their recent applications in load-bearing tissue. Polymers. 2018;10:1290.

28. Mahadik BP, Pedron Haba S, Skertich LJ, Harley BA. The use of covalently immobilized stem cell factor to selectively affect hematopoietic stem cell activity within a gelatin hydrogel. Biomaterials. 2015;67:297–307.

29. Gilchrist AE, Lee S, Hu Y, Harley BAC. Soluble signals and remodeling in a synthetic gelatin-based hematopoietic stem cell niche. Adv Healthc Mater. 2019;8:e1900751.

30. Bastianutto C, Mian A, Symes J, Mocanu J, Alajez N, Sleep G, et al. Local radiotherapy induces homing of hematopoietic stem cells to the irradiated bone marrow. Can Res. 2007;67:10112–6.

31. De Vita S, Li Y, Harris CE, McGuinness MK, Ma C, Williams DA. The gp130 cytokine interleukin-11 regulates engraftment of Vav1(-)(/)(-) hematopoietic stem and progenitor cells in lethally irradiated recipients. Stem Cells (Dayton, Ohio). 2018;36:446–57.

32. Waselenko JK, MacVittie TJ, Blakely WF, Pesik N, Wiley AL, Dickerson WE, et al. Medical management of the acute radiation syndrome: recommendations of the Strategic National Stockpile Radiation Working Group. Ann Intern Med. 2004;140:1037–51.

33. Hosing C. Hematopoietic stem cell mobilization with G-CSF. Methods Mol Biol (Clifton N J). 2012;904:37–47.

34. Nervi B, Link DC, DiPersio JF. Cytokines and hematopoietic stem cell mobilization. J Cell Biochem. 2006;99:690–705.

35. Drouet M, Hérodin F. Radiation victim management and the haematologist in the future: time to revisit therapeutic guidelines? Int J Radiat Biol. 2010;86:636–48.

36. Piau O, Brunet-Manquat M, L'Homme B, Petit L, Birebent B, Linard C, et al. Generation of transgene-free hematopoietic stem cells from human induced pluripotent stem cells. Cell Stem Cell. 2023;30:1610-23.e7.

37. Demirci S, Haro-Mora JJ, Leonard A, Drysdale C, Malide D, Keyvanfar K, et al. Definitive hematopoietic stem/progenitor cells from human embryonic stem cells through serum/feeder-free organoid-induced differentiation. Stem Cell Res Ther. 2020;11:493.

38. Magno V, Meinhardt A, Werner CJAFM. Polymer hydrogels to guide organotypic and organoid cultures. Adv Funct Mater. 2020;30:2000097.

39. Hughes CS, Postovit LM, Lajoie GA. Matrigel: a complex protein mixture required for optimal growth of cell culture. Proteomics. 2010;10:1886–90.

40. Yue K, Trujillo-de Santiago G, Alvarez MM, Tamayol A, Annabi N, Khademhosseini A. Synthesis, properties, and biomedical applications of gelatin methacryloyl (GelMA) hydrogels. Biomaterials. 2015;73:254–71.

41. Nichol JW, Koshy ST, Bae H, Hwang CM, Yamanlar S, Khademhosseini A. Cell-laden microengineered gelatin methacrylate hydrogels. Biomaterials. 2010;31:5536–44.

42. Mantel CR, O'Leary HA, Chitteti BR, Huang X, Cooper S, Hangoc G, et al. Enhancing hematopoietic stem cell transplantation efficacy by mitigating oxygen shock. Cell. 2015;161:1553–65.

43. Chen Y, Fang S, Ding Q, Jiang R, He J, Wang Q, et al. ADGRG1 enriches for functional human hematopoietic stem cells following ex vivo expansion-induced mitochondrial oxidative stress. J Clin Investig. 2021;131:e148329.

44. Ding L, Morrison SJ. Haematopoietic stem cells and early lymphoid progenitors occupy distinct bone marrow niches. Nature. 2013;495:231–5.

45. Ding L, Saunders TL, Enikolopov G, Morrison SJ. Endothelial and perivascular cells maintain haematopoietic stem cells. Nature. 2012;481:457–62.

46. Calvi LM, Adams GB, Weibrecht KW, Weber JM, Olson DP, Knight MC, et al. Osteoblastic cells regulate the haematopoietic stem cell niche. Nature. 2003;425:841–6.

47. Zhang J, Niu C, Ye L, Huang H, He X, Tong WG, et al. Identification of the haematopoietic stem cell niche and control of the niche size. Nature. 2003;425:836–41.

48. Nandakumar N, Mohan M, Thilakan AT, Sidharthan HK, Ramu J, Sharma D, et al. Bioengineered 3D microfibrous-matrix modulates osteopontin release from MSCs and facilitates the expansion of hematopoietic stem cells. Biotechnol Bioeng. 2022;119:2964–78.

49. Kara N, Xue Y, Zhao Z, Murphy MM, Comazzetto S, Lesser A, et al. Endothelial and Leptin Receptor(+) cells promote the maintenance of stem cells and hematopoiesis in early postnatal murine bone marrow. Dev Cell. 2023;58:348-60.e6.

50. Jang YY, Sharkis SJ. A low level of reactive oxygen species selects for primitive hematopoietic stem cells that may reside in the low-oxygenic niche. Blood. 2007;110:3056–63.

51. Ito K, Hirao A, Arai F, Matsuoka S, Takubo K, Hamaguchi I, et al. Regulation of oxidative stress by ATM is required for self-renewal of haematopoietic stem cells. Nature. 2004;431:997–1002.

52. Hu L, Yin X, Zhang Y, Pang A, Xie X, Yang S, et al. Radiation-induced bystander effects impair transplanted human hematopoietic stem cells via oxidative DNA damage. Blood. 2021;137:3339–50.

53. Shi MM, Kong Y, Song Y, Sun YQ, Wang Y, Zhang XH, et al. Atorvastatin enhances endothelial cell function in posttransplant poor graft function. Blood. 2016;128:2988–99.

54. Moroni M, Ngudiankama BF, Christensen C, Olsen CH, Owens R, Lombardini ED, et al. The Gottingen minipig is a model of the hematopoietic acute radiation syndrome: G-colony stimulating factor stimulates hematopoiesis and enhances survival from lethal total-body γ-irradiation. Int J Radiat Oncol Biol Phys. 2013;86:986–92.

55. Torisawa YS, Mammoto T, Jiang E, Jiang A, Mammoto A, Watters AL, et al. Modeling hematopoiesis and responses to radiation countermeasures in a bone marrow-on-a-chip. Tissue Eng Part C Methods. 2016;22:509–15.

56. van Os R, Robinson S, Sheridan T, Mauch PM. Granulocyte-colony stimulating factor impedes recovery from damage caused by cytotoxic agents through increased differentiation at the expense of self-renewal. Stem Cells (Dayton Ohio). 2000;18:120–7.

57. Li C, Lu L, Zhang J, Huang S, Xing Y, Zhao M, et al. Granulocyte colony-stimulating factor exacerbates hematopoietic stem cell injury after irradiation. Cell Biosci. 2015;5:65.

58. Zhang J, Ren X, Shi W, Wang S, Chen H, Zhang B, et al. Small molecule Me6TREN mobilizes hematopoietic stem/progenitor cells by activating MMP-9 expression and disrupting SDF-1/CXCR4 axis. Blood. 2014;123:428–41.

59. Liu Y, Ding L, Zhang B, Deng Z, Han Y, Wang S, et al. Thrombopoietin enhances hematopoietic stem and progenitor cell homing by impeding matrix metalloproteinase 9 expression. Stem Cells Transl Med. 2020;9:661–73.

Publisher's Note